Monthly Notices
of the
ROYAL ASTRONOMICAL SOCIETY

Mon. Not. R. Astron. Soc. **423,** 3049–3057 (2012) doi:10.1111/j.1365-2966.2012.21052.x

Metallicity effects on cosmic Type Ib/c supernovae and gamma-ray burst rates

V. Grieco,[1⋆] F. Matteucci,[1,2] G. Meynet,[3] F. Longo,[1] M. Della Valle[4] and R. Salvaterra[5]

[1] *Dipartimento di Fisica, Sezione di Astronomia, Università di Trieste, via G.B. Tiepolo 11, I-34131, Trieste, Italy*
[2] *INAF Osservatorio Astronomico di Trieste, via G.B. Tiepolo 11, I-34131, Trieste, Italy*
[3] *Observatory of the University of Geneva, CH1290 Versoix, Switzerland*
[4] *INAF Osservatorio Astronomico di Capodimonte, Salita Moiariello 16, 801313, Napoli, Italy*
[5] *INAF IASF-Milano, via Bassini 15, I-20133, Milano, Italy*

Accepted 2012 April 3. Received 2012 February 17; in original form 2011 September 15

ABSTRACT

Type Ib/c supernovae (SNe Ib/c) are likely to be associated with long gamma-ray bursts (GRBs), and therefore it is important to compare the SN rate in galaxies with the GRB rate. To do this we computed SN Ib/c rates in galaxies of different morphological types (ellipticals, spirals and irregulars) by assuming different histories of star formation and different SN Ib/c progenitors. We included some recent suggestions about the dependence of the minimum mass of single Wolf–Rayet (WR) stars on the stellar metallicity and therefore on galactic chemical evolution. We adopted several cosmic star formation rates (i.e. relative to a comoving unitary volume of the Universe) as a function of cosmic time, either observationally or theoretically derived, including the one computed with our galaxy models. We then computed the cosmic SN Ib/c rates. Our results show that the predicted SN Ib/c rates in spirals and irregulars can reproduce well the present observed rates if both single WR stars and massive binary systems are taken into account as SN Ib/c progenitors. The metallicity effects on the minimum mass for single WR stars are evident mainly in the early phases of galaxy evolution and do not influence substantially the predicted local Type Ib/c rates. We reached the following conclusions. (i) The ratio cosmic GRB rate /cosmic Type Ib/c rate varies in the range 10^{-2}–10^{-4} in the whole redshift range, thus suggesting that only a small fraction of all SNe Ib/c gives rise to GRBs. (ii) The metallicity dependence of SN Ib/c progenitors produces lower cosmic SN Ib/c rates at early times, for any chosen cosmic star formation rate. (iii) Different theoretical cosmic star formation rates, computed under different scenarios of galaxy formation, produce SN Ib/c cosmic rates that differ mainly at very high redshifts. However, it is difficult to draw firm conclusions on the high-redshift trend because of the large uncertainties in the data. (iv) GRBs can be important tracers of star formation at high redshifts if their luminosity function does not vary with redshift, and they can help in discriminating among galaxy formation models.

Key words: supernovae: general– galaxies: evolution – gamma-rays: bursts.

1 INTRODUCTION

Gamma-ray bursts (GRBs) are sudden and powerful gamma-ray flashes, occurring at a rate of ∼1 per day throughout the Universe. The duration of GRBs at MeV energies ranges from 10^{-3} to about 10^3 s, with long bursts being characterized by a duration >2 s. It has been established that some long GRBs are associated with supernovae (SNe) originating from the death of massive stars. These GRBs have been associated with powerful Type Ib/c supernovae (SNe Ib/c) having energies in excess of the majority of such SNe, and for this reason they have been called 'hypernovae' (Iwamoto et al. 1998; see also Paczyàski 1998). In particular, most of the evidence points towards SNe Ic (see Woosley & Bloom 2006; Hjorth & Bloom 2011). The 'collapsar' model proposed to explain long GRBs takes this phenomenological aspect into account and proposes a Wolf–Rayet (WR) progenitor that undergoes core collapse, producing a rapidly rotating black hole surrounded by an accretion disc that injects energy into the system and thus acts as a 'central engine' (Woosley 1993, MacFayden & Woosley 1999; Zhang, Woosley &

⋆E-mail: grieco@oats.inaf.it

MacFayden 2003). However, the collapsar can also originate in massive stars in binary systems, as suggested by several authors (e.g. Baron 1992; Kobulnicky & Fryer 2007; Yoon, Woosley & Langer 2010). Detailed galaxy evolution models are able to predict the temporal behaviour of SN rates in galaxies of all morphological types. Therefore, a comparison between theoretical SN Ib/c rates and observed GRB rates seems appropriate. Bissaldi et al. (2007) attempted such a comparison, but data on GRBs were not as readily available as they are now and were limited to lower redshifts. GRBs have now been observed up to $z \sim 8.2$ (Salvaterra et al. 2009a; Tanvir et al. 2009).

In this paper we aim to study the behaviour of the SN Ib/c rate in galaxies as a function of redshift and to compare it with the most recently derived cosmic GRB rate. In computing the SN Ib/c rate in galaxies we will adopt both single WR and massive binaries as GRB progenitors and will consider a dependence of the SN Ib/c progenitors on the initial stellar metallicity, which is not considered in any previous similar work (e.g. Bissaldi et al. 2007). Our intention is to make predictions for the rates of SN Ib/c at various redshifts in spiral and irregular galaxies. Currently, no observations can constrain such predictions, but in the future new powerful observational devices such as the James Webb telescope and the European Large Telescope (ELT) will provide extensive observational constraints on these rates. Comparisons with the present predictions will then allow us to confirm or reject the present predictions and will shed new light on the nature of the SN Ib/c progenitors and on the star formation histories in spiral and irregular galaxies. From the comparison between the observed GRB cosmic rate and the predicted cosmic SN Ib/c rate, we aim first to check whether the present ratio of GRBs to that of SN Ib/c can be well reproduced by our models and second to see how this ratio may change with redshift in the framework of our model.

In Section 2 we describe the chemical evolution model adopted to compute the evolution of galaxies of different morphological types, as well as the computation of the SN Ib/c rate. In Section 3 the computed SN Ib/c rates for irregular and spiral galaxies of various masses are presented and compared with the observed rates. In Section 4 we assemble various cosmic histories of star formation, including the one computed by means of our galaxy models, to compute the cosmic SN Ib/c rate, and then we compare this cosmic SN rate with the cosmic GRB rate. Finally, in Section 5 a discussion and some conclusions are presented.

2 THE CHEMICAL EVOLUTION MODELS

In order to compute the SN Ib/c rate in galaxies we need to know their star formation history. Galaxies of different morphological types (ellipticals, spirals, irregulars) are characterized by different star formation histories (see Matteucci 2001). In particular, ellipticals should have undergone an intense and short star formation episode, whereas spirals and irregulars should have had gentler star formation rates (SFRs) and are still forming stars now. Irregular galaxies must have had the mildest SFR because they contain more gas than galaxies of other types. Here, we focus on irregular and spiral galaxies for the following reasons: (i) SNe Ib/c are observed only in star-forming galaxies; and (ii) observations on the hosts of GRBs have revealed that long GRBs are associated with faint, blue and often irregular galaxies (Conselice et al. 2005; Fruchter et al. 2006; Tanvir & Levan 2007; Wainwright, Berger & Penprase 2007; Li 2008) and tend to occur in galaxies with low metallicities (Fynbo et al. 2003, 2006; Prochaska et al. 2004; Soderberg et al. 2004; Gorosabel et al. 2005; Berger et al. 2006; Savaglio 2006; Stanek et al. 2006; Wolf & Podsiadlowsky 2007; Modjaz et al. 2008; Savaglio, Glazebrook & Le Borgne 2009).

However, we do not exclude that this could be a selection effect (see e.g. Mannucci, Salvaterra & Campisi 2011; Campisi et al. 2011). In particular, Mannucci et al. (2011) suggest that the high-z/high-mass region is probably populated by dark GRBs. This idea is partially confirmed by observations of some dark GRB host galaxies provided by Krühler et al. (2011), wherein the masses of the dark GRB hosts seem to be higher than the masses of the normal GRB hosts.

We use a detailed self-consistent chemical evolution model reproducing the majority of the properties of irregular and spiral galaxies. Irregular galaxies play an important role in the study of chemical evolution and star formation owing to their simpler structure and lack of evolution compared with spiral galaxies. We also adopt a relatively simple model for spirals, neglecting gradients along the disc.

We assume that both irregular and spiral galaxies assemble all of their mass by means of a continuous infall of pristine gas. This is certainly true for spiral discs such as that of the Milky Way (see e.g. Chiappini, Matteucci & Gratton 1997; Chiappini, Matteucci & Romano 2001; Boissier & Prantzos 1999). The basic equations are

$$\dot{G}_i = -\psi(t)X_i(t) + R_i(t) + (\dot{G}_i)_{\rm inf} - \dot{G}_{i\rm w}(t), \quad (1)$$

where $G_i(t) = M_{\rm gas}(t)X_i(t)/M_{\rm inf}$ is the gas mass in the form of an element i normalized to the present-time total luminous infall mass. The quantity $X_i(t) = G_i(t)/G(t)$ represents the abundance by mass of an element i, and by definition the summation over all the elements present in the gas mixture is equal to unity. The quantity $G(t) = M_{\rm gas}(t)/M_{\rm inf}$ is the total fractional mass of gas. The quantity $R_i(t)$ represents the rate at which the element i is restored into the interstellar medium (ISM) by the dying stars. Finally, $(\dot{G}_i)_{\rm inf}$ and $\dot{G}_{i\rm w}(t)$ represent the infall and wind rate, respectively.

The SFR ($\psi(t)$), namely the amount of interstellar gas, expressed in solar masses, turning into stars per unit time, is assumed to be continuous and defined as a Schmidt (1959) law:

$$\psi(t) = \nu G(t), \quad (2)$$

where the quantity ν is the star formation efficiency (SFE), namely the inverse of the typical time-scale for star formation, and is expressed in $\rm Gyr^{-1}$. The SFE for spirals is assumed to be higher than that for irregulars. We explored one initial mass functions (IMF), namely the Salpeter (1955) one ($x = 1.35$ in the mass range 0.1–$100\,\rm M_{\odot}$).

A main assumption of the model for irregulars is the existence of galactic winds triggered by SN explosions. In particular, it is assumed that a fraction (∼30 per cent) of the initial blast wave energy of SNe is transformed into thermal gas energy and the wind starts when the thermal energy of the gas equates to the binding energy of the gas. The wind can be 'normal', namely each element is lost at the same rate, or 'differential', in the sense that some elements (metals for example) are lost preferentially (see Bradamante, Matteucci & D'Ercole 1998). A galactic wind is likely to occur in these systems because of their relatively low potential well. Moreover, galactic outflows are observed in irregular galaxies (see e.g. Martin 1999; Martin, Kobulnicky & Heckman 2002). In order to consider a galactic wind we follow the method described in Bradamante et al. (1998) and Yin et al. (2010); in particular, the wind rate is assumed to be proportional to the SFR through a free parameter λ_i larger than zero:

$$\dot{G}_{i\rm w}(t) = \lambda_i \psi(t), \quad (3)$$

where i represents a specific chemical element. To have a preferential loss of metals, as indicated by dynamical models (e.g. Mac Low & Ferrara 1999), we use a differential wind in which $\lambda_{\rm H} = \lambda_{\rm He} = 0.3$ and $\lambda_i \sim 0.9$ for the other elements.

In the case of spirals, a galactic wind is less likely to occur, owing to the deep potential well in which the spiral discs lie. In fact, spiral discs are more likely to have galactic fountains than galactic winds (Spitoni et al. 2009).

Finally, the assumed rate of infall is the same for irregulars and spirals and follows the law

$$(\dot{G}_i)_{\rm inf} = \frac{a(X_i)_{\rm inf}\, {\rm e}^{-t/\tau}}{M_{\rm inf}}, \quad (4)$$

where a is a suitable constant, derived by integrating equation (3) over the galactic lifetime, $(X_i)_{\rm inf}$ is the abundance by mass of the element i in the infalling gas, assumed to be primordial, and τ is the infall time-scale. This time-scale is expressed in Gyr and is defined as the characteristic time at which half of the total mass of the system has assembled. The values of τ are derived as the ones best able to reproduce the majority of the observational constraints. This time-scale is different for galaxies of different morphological types, being quite short in spheroids and increasing for spirals and irregulars.

In Table 1 we show the adopted model parameters for a typical spiral galaxy (Milky Way-like) and for a typical irregular galaxy. The infall mass $M_{\rm inf}$ is the mass that eventually would be accreted if there was no galactic wind. Model Irr is described by an infall mass of $5 \times 10^9\,{\rm M}_\odot$, which is one order of magnitude lower than the infall mass of Model Sp. The infall time-scale for the spiral galaxy is assumed to be 6 Gyr, although in the Milky Way disc the time-scale for disc formation is shorter in the internal than in the external regions (inside-out formation, Matteucci & François 1989; Chiappini et al. 1997); here we only want to show some averaged properties, and 6 Gyr is an average time-scale between the internal (∼2 Gyr) and external (∼10–12 Gyr) time-scale. The time-scale for the formation of irregulars is assumed to be shorter (4 Gyr). In Table 1 we report the wind parameter for irregular galaxies (λ_i, equation 3) and the SFE for irregulars and spirals. Following the work of Calura et al. (2009), we assume that the SFE increases with galactic mass.

Finally, in order to compute the cosmic star formation rate (CSFR) and SN Ib/c rate we also consider a model for a typical elliptical of 10^{11} luminous mass. This model predicts a short and intense burst of star formation that stops before 1 Gyr, owing to the occurrence of strong galactic winds that empty the galaxy of gas. The SFE adopted for this elliptical is $10\,{\rm Gyr}^{-1}$, implying that this galaxy assembles more quickly than the late-type ones. The assumed IMF is the Salpeter one, as assumed for the other galaxy types. It is worth noting that this model, as well as the other models

Table 1. Parameter sets used for describing our models: $M_{\rm inf}$ is the final total assembled mass if nothing is lost, τ is the infall time-scale, λ_i is the wind parameter (see equation 3) and SFE is the star formation efficiency.

	Model Irr	Model Sp
$M_{\rm inf}$ [M$_\odot$]	5×10^9	5×10^{10}
τ [Gyr]	3	6
λ_i	Differential	No wind
SFE [Gyr^{-1}]	0.05	2

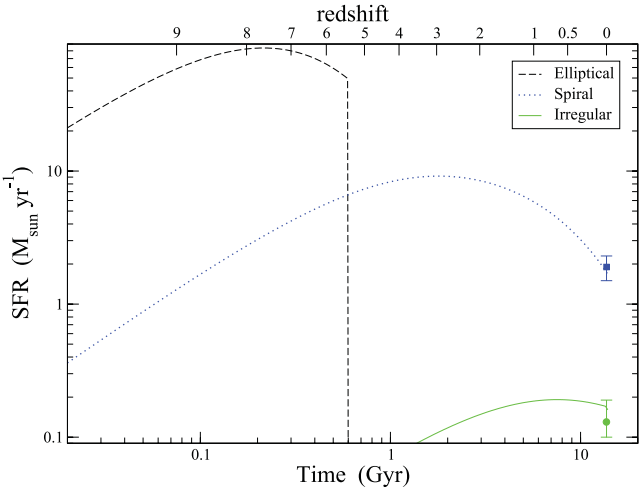

Figure 1. Predicted star formation rates of typical elliptical, spiral and irregular galaxies, expressed in ${\rm M}_\odot\,{\rm yr}^{-1}$, as functions of time and redshift; the redshift of galaxy formation is $z_{\rm f} = 10$ in a ΛCDM cosmology. The infall masses for each type of galaxies are: $10^{11}\,{\rm M}_\odot$ (elliptical, dashed line), $5 \times 10^{10}\,{\rm M}_\odot$ (spiral, dotted line) and $5 \times 10^9\,{\rm M}_\odot$ (irregular, solid line). Also shown are some average values for the present-time star-formation rate in spirals (square, Chomiuk & Povich 2011) and in irregulars (circle, Harris & Zaritsky 2009).

for spirals and irregulars, well reproduces the local properties of ellipticals (Calura & Matteucci 2004; Pipino & Matteucci 2004). The star formation history of this elliptical is shown in Fig. 1, together with the SFRs of a spiral and an irregular galaxy.

2.0.1 Nucleosynthesis and stellar evolution prescriptions

In order to compute the chemical evolution of these galaxies, in particular the evolution of the O abundance, we adopted the yields from massive stars given in Woosley & Weaver (1995), the yields from low- and intermediate-mass stars in van den Hoek & Groenewegen (1997), and the yields from SNe Ia in Iwamoto et al. (1999, their model W7). Concerning the progenitors of SNe Ib/c, it has been suggested that they could be single WR stars, namely stars that have lost most of their H and He envelope and with masses larger than $M_{\rm WR}$, which depends on the initial stellar metallicity. In fact, the mass loss in massive stars ($M \geq 10\,{\rm M}_\odot$) increases with the initial metallicity in the way that $M_{\rm WR}$ decreases with increasing metallicity (see Tables 2, 3). In other words, with a high rate of mass loss, even stars of 20–25 M$_\odot$ can become WRs. However, the progenitors of SNe Ib/c could also be massive stars in binary systems in the mass range 12–20 M$_\odot$ (e.g. Baron 1992; Bissaldi et al. 2007) or 14.8–45 M$_\odot$ (Yoon et al. 2010). Here we consider both progenitors (see Smartt 2009), following in part the work of Bissaldi et al. (2007) but adopting recent prescriptions for the dependence of $M_{\rm WR}$ on metallicity and a mass range of 14.8–45 M$_\odot$

Table 2. Relation between the minimal Wolf–Rayet mass able to form SNe Ib/c and metallicity, for various ranges of metallicity.

$M_{\rm WR} - Z$ relation	Z range	$M_{\rm WR}({\rm M}_\odot)$
$M_{\rm WR} = -15290Z + 113.76$	$Z \leq 0.004$	∼52.6 M$_\odot$ @ $Z = 0.004$
$M_{\rm WR} = -5650Z + 75.20$	$0.004 < Z \leq 0.008$	∼30 M$_\odot$ @ $Z = 0.008$
$M_{\rm WR} = -416.5Z + 33.33$	$0.008 < Z < 0.02$	∼27.7 M$_\odot$ @ $Z = 0.0134$
$M_{\rm WR} = -230Z + 29.6$	$0.02 \leq Z \leq 0.04$	∼25 M$_\odot$ @ $Z = 0.020$
$M_{\rm WR} = 20\,{\rm M}_\odot$	$Z > 0.04$	∼20.4 M$_\odot$ @ $Z = 0.040$

Table 3. Relation between the minimal Wolf–Rayet mass able to form SNe Ic and metallicity, for various ranges of metallicity.

$M_{\rm WR} - Z$ relation	Z range	$M_{\rm WR}(\rm M_\odot)$
$M_{\rm WR} = -10759Z + 116$	$Z \leq 0.008$	$\sim 30\,\rm M_\odot$ @ $Z = 0.008$
$M_{\rm WR} = 750Z + 24$	$0.008 < Z < 0.02$	$\sim 34\,\rm M_\odot$ @ $Z = 0.0134$
$M_{\rm WR} = -700Z + 53$	$0.02 \leq Z \leq 0.04$	$\sim 39\,\rm M_\odot$ @ $Z = 0.02$
$M_{\rm WR} = 25\,\rm M_\odot$	$Z > 0.04$	$\sim 25\,\rm M_\odot$ @ $Z = 0.04$

for the total mass of binary systems. In particular, we consider the results of Georgy et al. (2009), which give the variation of $M_{\rm WR}$ as a function of the metallicity for all the core-collapse SNe. In Tables 2 and 3 we show the $M_{\rm WR}$–Z relations extrapolated from the results of Georgy et al. (2009) and adapted to the metallicity range of our galactic models for SN Ib/c and only Ic progenitors, respectively. In particular, in column 1 we show the relation between the minimum WR mass and metallicity for a range of Z-values, indicated in the second column. Finally, in the third column we show the minimum WR mass corresponding to specific metallicities.

2.1 The computation of the SN Ib/c rate

The distinguishing features of Type Ib and Ic SNe is the lack of conspicuous hydrogen spectral lines. SNe Ib/c occur preferentially in the vicinity of star-forming regions, and their progenitors are thought to be massive stars that have lost most of their H-rich (and perhaps their He-rich) envelopes through strong winds or transfer to a binary companion via Roche overflow. Approximately 25 per cent of all core-collapse SNe fall in the SNe Ib and SNe Ic category (Hamuy 2002).

The SN Ib/c and SN Ic rates have been calculated assuming both single WRs and stars in close binary systems as progenitors. In general,

$$SNR = \int_{M_{\rm WR}}^{100} \psi(t - \tau_M)\phi(M)\,{\rm d}M + F\int_{14.8}^{45} \psi(t - \tau_M)\phi(M)\,{\rm d}M \sim \psi(t)\Big[\int_{M_{\rm WR}}^{100} \phi(M)\,{\rm d}M + F\int_{14.8}^{45} \phi(M)\,{\rm d}M\Big], \quad (5)$$

where the lifetime τ_M of massive stars is considered negligible, $\psi(t)$ is the star formation rate and $\phi(M)$ is the IMF. The same equation is used for both SNe Ib/c and SNe Ic alone, the only difference being in the minimum stellar mass of the progenitors, $M_{\rm WR}$, varying as shown in Table 2 for the SNe Ib/c and in Table 3 for the SNe Ic. Concerning SNe Ib/c, in one case the evolution of $M_{\rm WR}$, shown in Fig. 3, is taken into account, while in the other case $M_{\rm WR}$ is assumed to be independent of metallicity and to be $25\,\rm M_\odot$. Because, in this last case, the evolution of the SNR is the same for both the SN types, we do not show the evolution of SNe Ic with $M_{\rm WR}$ constant. The factor F represents the fraction of massive binary stars producing SNe Ib/c. For the moment, this parameter is chosen to be equal to 0.15 (Calura & Matteucci 2006). The choice of this value is motivated by the fact that first, in any galaxy, half of the massive stars are possibly in binary systems, and second, the fraction of massive stars in close binary system is ∼30 per cent, that is, similar to the close binary frequency predicted for low-mass systems (Jeffries & Maxted 2005). Therefore, the estimated value for this parameter is given by $F \sim 0.5 \times 0.3 \sim 0.15$. This is in good agreement with Podsiadlowski, Joss & Hsu (1992), who calculated that 15–30 per cent of all massive stars (with initial masses above $8\,\rm M_\odot$) could conceivably transfer mass to an interacting companion and end up as helium stars. However, we have also tested other values of the F parameter: in particular, for spirals we ran models with F in the range 0.01–0.5 and found that the error on the predicted present SN Ib/c rate is ∼0.003 SNe yr^{-1}, while for irregulars we ran models with F in the range 0.01–0.3 (the value of 0.5 gives present SN Ib/c rates too high relative to observations) with an error in the theoretical SN Ib/c rate of ∼0.0003 SNe yr^{-1}. We can safely conclude that in both cases F-values lower than 0.15 are not high enough to reproduce the observed SN Ib/c rates (see next paragraph), whereas higher but not unreasonable values (up to $F = 0.5$) do not produce sensible differences in the results. Therefore, we do not exclude that our chosen value of F could be a lower limit.

3 RESULTS

Before comparing model results with the observed properties of galaxies, we summarize some observational facts that are used to constrain our models as follows.

(i) The total fractional mass of gas in irregulars is

$$(M_{\rm gas}/M_{\rm tot})_{t\sim 13\,\rm Gyr} = [0.2 - 0.8],$$

whereas in spirals it is

$$(M_{\rm gas}/M_{\rm tot})_{t\sim 13\,\rm Gyr} < 0.3.$$

(ii) The global average metallicity in irregulars is

$$Z(t \sim 13\,\rm Gyr) = [0.03 - 0.5]\,Z_\odot,$$

whereas the average metallicity in the disc of a Milky Way-like spiral is

$$Z(t \sim 13\,\rm Gyr) = [2 - 2.5]\,Z_\odot,$$

where $Z_\odot \sim 0.0134$ (Asplund et al. 2009).

(iii) The stellar mass versus metallicity relation is an important observational constraint both for spirals and for irregulars. In particular, the relation for irregulars seems to be the lower part of the relation for spirals. The mass–metallicity relation indicates that the stellar mass of star-forming galaxies is correlated with the galaxy metallicity: galaxies with larger stellar masses tend to have higher metallicities (Tremonti et al. 2004, Savaglio et al. 2005; Erb et al. 2006; Kewley & Ellison 2008: Maiolino et al. 2008).

(iv) The predicted SN Ib/c rate ($SNR_{Ib/c}$) should reproduce the following observational rates provided by Li et al. (2011):

$$SNR_{Ib/c} = 0.103^{+0.136}_{-0.067} SNuM \text{ (Irregulars)},$$

$$SNR_{Ib/c} = 0.113^{+0.031}_{-0.025} SNuM \text{ (Spirals)},$$

where $SNuM = SNe(100\,\rm yr)^{-1}(10^{10}\,\rm M_\odot)^{-1}$ is the SN Ib/c rate per unit mass, in good agreement with previous works (i.e. Mannucci et al. 2005). These observed rates can therefore be computed for galaxies of the same stellar mass as in our models and compared with our predicted rates.

The predicted values at the present time of the total metallicity (Z), total fractional mass of gas in the galaxy ($M_{\rm gas}/M_{\rm tot}$), stellar mass in solar units ($M_{\rm star}$) and oxygen abundance [expressed as $\log(O/H) + 12$] are shown in Table 4. It should be noted that the values of Z and 12+ log(O/H) for the spiral galaxy are larger than solar: the reason is that they represent the average metallicities over the entire galactic disc, where the inner regions have over-solar values and the external ones have lower values.

Table 4. Predictions of Model Irr and Model Sp at the present time: the total metallicity, total fractional mass of gas in the galaxy, stellar mass, oxygen abundance and star formation rate.

	Model Irr	Model Sp
Z	0.0096	0.03
$(M_{\rm gas}/M_{\rm tot})_{t\sim 13\,{\rm Gyr}}$	0.66	0.017
$M_{\rm star}$ [$M_\odot$]	1.4×10^9	4.27×10^{10}
$12 + \log(O/H)$	8.6	9.12
SFR [$M_\odot$ yr^{-1}]	0.16	1.67

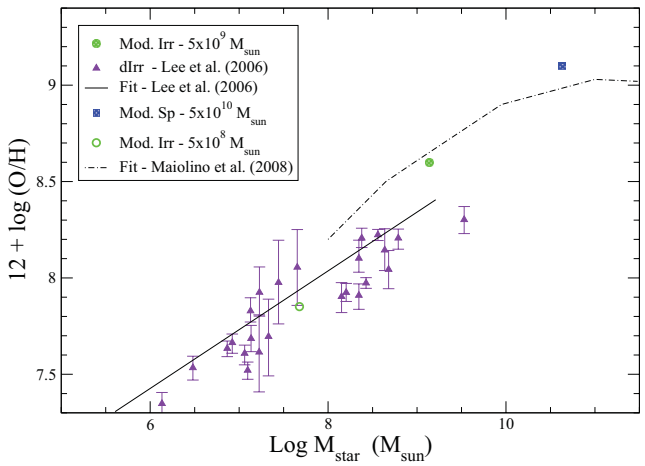

Figure 2. Predicted and observed mass–metallicity relations for irregular galaxies; the dot-dashed curve represents the best fit to the data of Maiolino et al. (2008) regarding star-forming galaxies, and the solid curve the best fit to the data obtained by Lee et al. (2006) for a sample of local dwarf galaxies (purple triangles). The symbols are the predictions for Model Irr (green circles) and Model Sp (blue square). For the irregulars we also show a model with infall mass $M_{\rm inf} = 5 \times 10^8$ and SFE = 0.02 (open green circle).

We see that present models provide values in agreement with observations for the present total mass fraction of gas and for the average metallicity in both types of galaxies considered here.

In Fig. 1, the time evolution of the star formation rates (expressed in $M_\odot$ yr^{-1}) is plotted for the three types of galaxies (elliptical, spiral and irregular). The SFR increases until the energy injected into the ISM by stellar winds and SN(Ia, Ib and II) explosions triggers a galactic wind. At that time, the thermal energy is equivalent to the binding energy of the gas, and the gas is lost at a rate proportional to the SFR (equation 3) with a consequent drop of the SFR. Furthermore, we can see that the present models fit the present-time averaged SFR well both in spirals and in irregulars.

Fig. 2 shows the predicted and observed mass–metallicity relations at the present time for low-mass galaxies. In particular, we show both the best fit of Maiolino et al. (2008) of the data provided by Kewley & Ellison (2008) concerning star-forming galaxies, and the data and best fit of dwarf irregulars as inferred by Lee et al. (2006). As can be seen, our models lie close to the best fits. In our galaxy models the mass–metallicity relation arises naturally by adopting a smaller SFE in smaller galaxies. The above comparisons show that our chemical models reproduce very well many observed properties of present-day spirals and irregulars. Because these present-day properties result from the whole previous evolution, this good correspondence gives confidence that these models can be used to explore the much less well-known early phases of

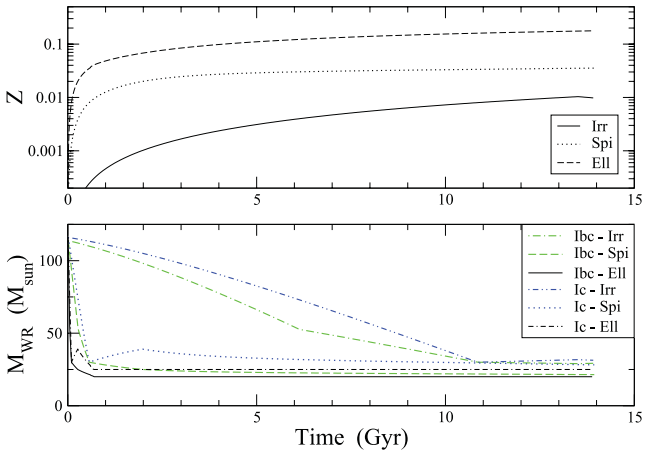

Figure 3. Upper panel: evolution of the total metallicity as a function of time for Model Irr (solid line), Model Sp (dotted line) and for a typical elliptical (dashed line). Lower panel: evolution of the minimal mass of Wolf–Rayet progenitors as a function of time for SN Ibc and SN Ic in Model Irr (green dotted–dashed line and blue double-dotted–dashed line), Model Sp (green dashed line and blue dotted line) and for a typical elliptical (black solid line and black double-dashed–dotted line).

these galaxies, which should be observed in greater detail in the near future thanks to more powerful observational devices such as the James Webb telescope and the ELT.

In Fig. 3 we show the evolution of the metallicity Z for our galaxies and the corresponding evolution of the minimum WR mass, according to the relations of Table 2 and 3. As can be seen, owing to the gentler increase of metallicity in the irregular galaxy, $M_{\rm WR}$ varies more gradually as a function of time in this galaxy than in the spiral one. On the other hand, the variation of $M_{\rm WR}$ in an elliptical is very fast in the very early phases.

In Fig. 4, the SN Ib/c and Ic rates are shown as a function of time for Model Irr and Model Sp. Different rates arise under different assumptions concerning the SN Ib/c and SN Ic progenitors and their dependence on the initial stellar metallicity (see Section 2.1). The percentage of SNe from binary systems represents ∼30 per cent of the total predicted rate. The symbols in Fig. 4 are the observed SN Ib/c rates for an irregular (circle) and a spiral (square) galaxy provided by Li et al. (2011).

It is worth noting that the samples of SN-host galaxies usually include (owing to an observational bias) small numbers of irregulars. Following Li et al. (2011), one can conservatively assume that the true value of the SN rate in irregulars is between the Li et al. (2011) and Mannucci et al. (2005) estimates. In Fig. 4 this uncertainty is included in the size of the error bars.

As can be seen, the predicted present-time rates of SNe Ib/c are consistent, within the error bars, with the observed ones.

An interesting quantity, often shown in the literature, is the ratio between the SN Ib/c and the SN II rate, $N_{\rm Ibc}/N_{\rm II}$ (e.g. Prantzos & Boissier 2003; Boissier & Prantzos 2009; Prieto, Stanek & Beacom 2008; Smartt 2009; Smith et al. 2011). In order to have a more consistent comparison with the data we have plotted the $N_{\rm Ibc}/N_{\rm II}$ and $N_{\rm Ic}/N_{\rm II}$ ratios as functions of metallicity (see Fig. 5). It is worth noting that when using $N_{\rm Ibc}/N_{\rm II}$ and $N_{\rm Ic}/N_{\rm II}$ versus metallicity, we cannot specify the galaxy type because the relation between mass, metallicity and IMF is the same for all galaxy types. As can be seen from Fig. 5, our predictions are in good agreement with the data in the case of both SNe Ib/c (solid line) and SNe Ic

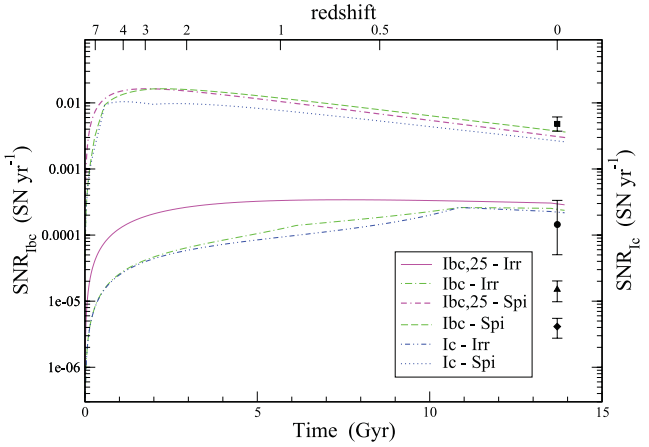

Figure 4. SN Ib/c and Ic rates as a function of time and redshift for Model Irr (magenta solid line, green dotted–dashed line and blue double-dotted–dashed line) and Model Sp (dotted–double-dashed magenta line, green dashed line and blue dotted line). The redshift of galaxy formation is $z_f = 10$ in a ΛCDM cosmology. The various model predictions for each rate depend on the assumptions concerning the SN Ib/c and SN Ic progenitors and their dependence on the initial stellar metallicity: $M_{WR} = 25\,M_\odot$ (solid line for Model Irr and dotted–double-dashed line for Model Sp), $M_{WR} = M(Z)$ (dashed line for SN Ibc and dotted line for SN Ic in Model Sp; dashed–dotted line for SN Ibc and double-dotted–dashed line for SN Ic in Model Irr). The symbols are the observed SN Ib/c rates, obtained by multiplying the observed rate per unit mass (Li et al. 2011) by the present-time stellar mass of the galaxy in Model Irr (circle) and Model Sp (square). Also shown is the local GRB rate provided by Guetta, Piran & Waxman (2005), triangle, and Salvaterra et al. (2012), diamond.

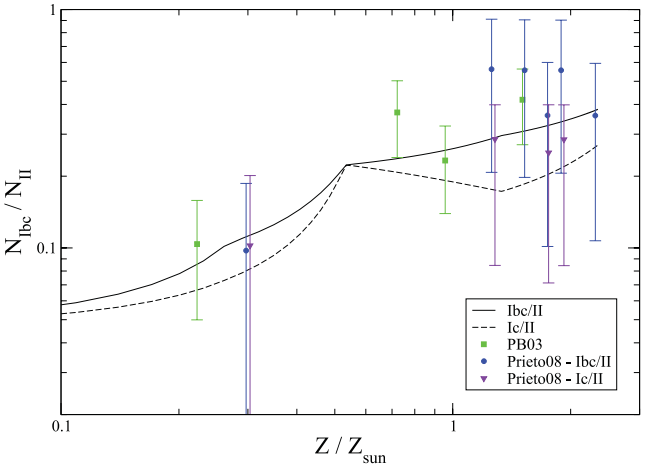

Figure 5. Number ratio of SN Ib/c and Ic to SN II as a function of metallicity of the host galaxy (solid and dashed lines, respectively). The circles and the inverted triangles are the values obtained by Prieto et al. (2008) from directly measured central metallicities for SN Ibc and SN Ic, respectively, while the squares are the results from Prantzos & Boissier (2003) using absolute magnitudes as a proxy to host metallicities.

(dashed line) and with previous calculations (Boissier & Prantzos 2009).

4 THE LOCAL GRB/SN$I_{b/c}$ RATIO

Fig. 4 shows the good match between the 'expected' SN Ib/c 'local' rate, computed for spirals and irregulars, and the 'observed' SN rates derived by Li et al. (2011). This agreement assesses quantitatively the reliability of the prescriptions that have been used in Sections 2 and 3 to derive the SN Ib/c rate as a function of time and gives more weight to the results that will be presented in Section 5. When the metallicity effect on the minimum WR mass is taken into account, there is a difference only for irregulars, mainly at early times, owing to the slower growth of metallicity in these systems.

It is interesting to compute the ratio of SNe Ib/c to GRBs (in the local Universe), and to do this we compare the theoretical SN Ib/c rates, shown in Fig. 4, with the local rate of GRBs at the present time (triangle). The 'canonical' value for the latter quantity ranges between ~ 0.5 GRB Gpc^{-3} yr^{-1} (Schmidt 2001) and $\sim$1 event Gpc^{-3}yr^{-1} (Guetta et al. 2005). In order to compare the SN Ib/c and the GRB rate in the right units we use the local GRB rate of 1.1 events Gpc^{-3}yr^{-1} (Guetta et al. 2005), taking into account the local density of B luminosity, $\sim 1.2 \times 10^8\ L_{B,\odot}$ Mpc^{-3} (e.g. Madau, Della Valle & Panagia 1998) and the B luminosity of the Milky Way, $2.3 \times 10^{10}\ L_{B,\odot}$. This approach gives $R_{GRB} \sim 2.1 \times 10^{-7}$ yr^{-1}. This 'observed' rate has to be re-scaled by using the beaming factor, f_b^{-1}. The beaming factor accounts for the fact that a GRB does not light up the full celestial sphere but rather a fraction of it. There are several estimates of this parameter: $f_b^{-1} \leq 10$ (Guetta & Della Valle 2007) for local and low-luminosity GRBs, corresponding to $\theta > 25^\circ$, and $f_b^{-1} \sim 75500$ (Guetta et al. 2005, Yonetoku et al. 2005; van Putten & Regimbau 2003, Frail et al. 2001), for high-luminosity GRBs, corresponding to beaming angles of $\sim(10^{-4})^\circ$.

If we conservatively assume, for 'local' GRBs, $f_b^{-1} \leq 75$, we derive a 'local' ratio GRB/SN Ib/c of $\leq 3 \times 10^{-3}$ and $\leq 2 \times 10^{-2}$ in spirals and irregulars, respectively. This is an expected result, as not all SNe Ib/c will end up as long GRBs.

In Fig. 4 we show the GRB rate provided by Guetta et al. (2005) in units of yr^{-1} and re-scaled using the beaming factor $f_b^{-1} = 75 \pm 25$.

5 THE COSMIC SN$I_{b/c}$ AND GRB RATES

The cosmic SN and GRB rates are defined in a unitary comoving volume of the Universe. This definition is necessary to study the rates at high redshifts, where the morphology of the observed galaxies is not known. The cosmic rates refer, in fact, to a mixture of galaxies that can be different at every redshift. Both the cosmic Type Ib/c and GRB rates depend on the SFR in galaxies but also on the galaxy and GRB luminosity functions. If these functions do not evolve with redshift then both the SN and the GRB rate will trace the CSFR. In contrast, the observed behaviour can be caused by the evolution of the luminosity functions of galaxies (e.g. number density evolution). The CSFR has now been measured up to very high redshifts ($z \sim 8$), in particular thanks to galaxies hosting GRBs (see Kistler et al. 2009). In Fig. 6, we show a revised version of the CSFR predicted by Calura & Matteucci (2003) and obtained by taking into account the evolution of galaxies of different morphological types (ellipticals, spirals and irregulars), as described in the previous sections. In particular, the CSFR has been computed by assuming a pure luminosity evolution of galaxies; in other words, the main parameters of the Schechter (1976) galaxy luminosity function have been kept constant with redshift. To compute the CSFR we adopted the following relationship:

$$CSFR = \sum_k \psi_k(t)\, n_k^* \quad [M_\odot\ \mathrm{yr}^{-1}\,\mathrm{Mpc}^{-3}], \tag{6}$$

where k identifies a particular galaxy type (elliptical, spiral, irregular), and $\psi_k(t)$ represents the history of star formation in each galaxy, as shown in Fig. 1. The quantity n_k^* is the galaxy number density,

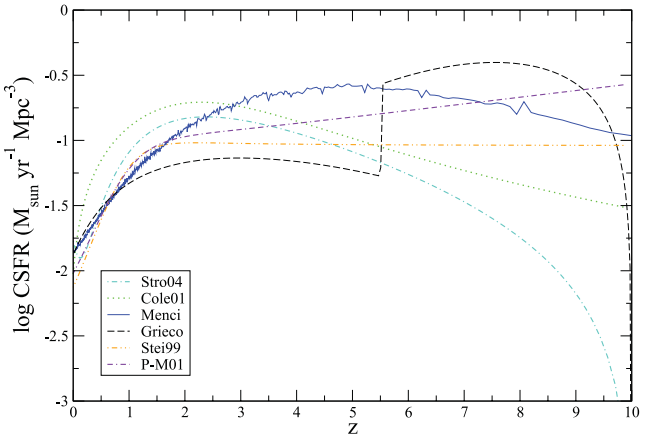

Figure 6. Evolution of various cosmic star formation rates with redshift: Menci (private communication) (blue solid line), our model (black long-dashed line), Strolger et al. (2004) (turquoise dashed–dotted line), Steidel et al. (1999) (orange double dotted-dashed line) and Porciani & Madau (2001) (violet double-dashed–dotted line). The green dotted line is the fit (Cole et al. 2001) of the data collected by Hopkins (2004): this fit has been extended up to redshift $z = 6$.

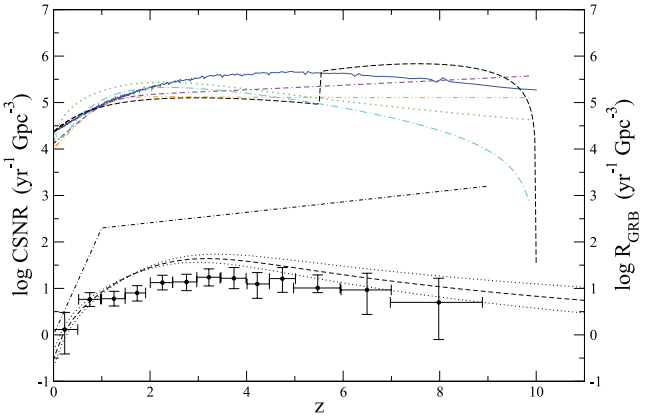

Figure 7. Comparison between the cosmic predicted SN Ib/c rates computed by means of all the CSFRs of Fig. 6 and the number of observed GRBs at various redshifts provided by Wanderman & Piran (2010), Swift data (black circles with error bars) and Matsubayashi et al. (2005) (black dashed–dotted line in the lower part of the figure). The short-dashed and the double-dotted black lines, below the Matsubayashi et al. (2005) rate, represent the best fit and the upper and lower limits, respectively, of the cosmic GRB rate obtained by Salvaterra et al. (2012). The Ib/c CSFRs are computed by means of the CSFRs shown in Fig. 6 and are indicated with the same symbols.

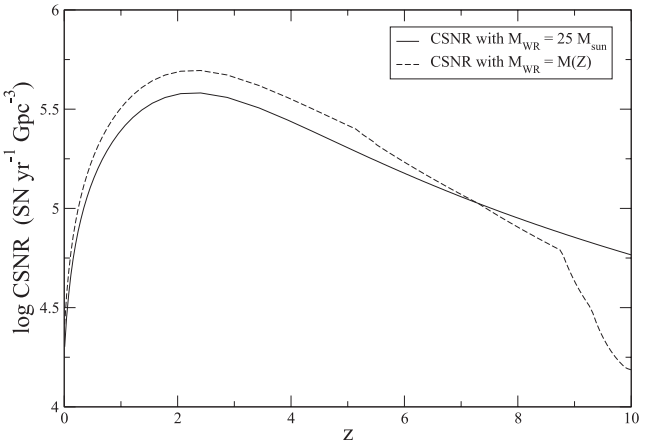

Figure 8. Comparison between the cosmic predicted SN Ib/c rates computed by means of the CSFR of Cole et al. (2001) and with various assumptions on M_{WR}: the solid line refers to a constant M_{WR} whereas the dashed line refers to the case of $M_{WR} = M(Z)$.

expressed in units of Mpc^{-3} for each morphological galaxy type and has been assumed to be constant and equal to the present-time value, as derived by Marzke et al. (1994). This CSFR is therefore obtained by assuming that all galaxies started forming stars at the same time and that there is no number density evolution; these are very simple assumptions but can be useful to disentangle the effect of the SFR from that of the luminosity function and to compare these results with predictions from hierarchical galaxy formation models. This predicted CSFR shows a high peak of star formation at very high redshifts owing to the contribution of the ellipticals that formed their stars very early. This predicted high-redshift CSFR is probably too high and unrealistic, as the number density of ellipticals at high redshifts could have been overestimated. In other words, the hypothesis of no number density evolution could be incorrect. On the other hand, the predicted CSFR for redshift $z < 6$ seems underestimated relative to the data. This does not mean that our galactic SF histories are wrong, but again the discrepancy could be caused by neglecting the number density evolution of galaxies. We have also adopted CSFRs computed in the framework of the hierarchical clustering galaxy formation scenario, as well as the fit to the observed CSFR. In fact, Fig. 6 also shows the CSFR obtained by Cole et al. (2001) best fitting the data collected by Hopkins (2004) from 1995 onwards. This same parametric form has been used subsequently by many authors such as Hopkins & Beacom (2006) and Blanc & Greggio (2008), as it also fits more recent data up to redshift $z = 6$.

It is worth noting that all the other theoretical CSFRs shown in Fig. 6 underestimate the CSFR at intermediate and low redshifts. To derive the CSFR observationally one should adopt some of the well-known tracers of SF, in particular H_α, H_β, UV continuum. In these wavebands the effect of dust cannot be neglected and therefore the dust correction is necessary to obtain the correct CSFR. The differences between corrected and uncorrected data are generally large, as shown by Strolger et al. (2004). In particular, uncorrected data tend to show a strong decline of the CSFR for $z > 2$, whereas the corrected data show an almost constant CSFR for $z > 3$. Another important effect in the derivation of the CSFR is related to the uncertainty at the faint end of the luminosity function of galaxies.

By means of these various CSFRs we computed the cosmic SN Ib/c rate shown in Fig. 7, which also reports the observed cosmic GRB rate. The adopted progenitors for SNe Ib/c are assumed to be single WR stars with a constant minimum mass of 25 $M_\odot$ plus binary systems, as described in Section 2.1. As it can be seen, the theoretical error in the CSFR, and consequently in the CSNR, increases towards high and very high redshifts and is roughly a factor of 10 at $z = 6$. Clearly at these high redshifts ($z > 6$) the uncertainties are still too large to draw any conclusion. In Fig. 8 we show the predicted cosmic SN Ib/c rate obtained by adopting the Cole et al. (2001) CSFR and M_{WR} depending on Z, all the other assumptions remain the same. Here we have considered the cosmic evolution of Z, and in particular we assumed the Z versus time evolution typical of an elliptical galaxy of 10^{11} $M_\odot$ as shown in Fig. 3; this is because by weighting the Z versus time of each galaxy on

their number density, the Z versus time relation of the ellipticals dominates at all redshifts. In fact, spheroids are very likely to be responsible for the production of the bulk of metals in the Universe (see Calura & Matteucci 2004). As can be seen in Fig. 8, the effect of metallicity on the SN Ib/c progenitors is stronger at early times and produces a lower cosmic SN Ib/c rate. This effect would be similar if applied to all the CSFRs of Fig. 6

Coming back to Fig. 7, a visual inspection of this figure confirms that GRBs originating from the explosion of massive stars account for only a tiny fraction of the SNe Ib/c class. In particular, the comparison of the SN Ib/c rates with the Matsubayashi et al. (2005) semi-empirical track suggests the ratio GRB/SN Ib/c to be $\sim 10^{-4}$ in the local Universe and to increase up to $\sim 10^{-3}$–10^{-2} over the redshift range $z = 1$–8. Interestingly, the GRB/SN Ib/c ratio at $z \sim 0$ nicely reproduces the 'observed' ratio between the local GRB rate and the SN Ib/c rates obtained by other authors: ~ 1 GRB Gpc^{-3} yr^{-1} (Guetta et al. 2005) and $\sim 2 \times 10^4$ SN Ib/c Gpc^{-3} yr^{-1} (Guetta & Della Valle 2007), respectively. Taking these figures at face value, we conclude that 'local' and 'low-luminosity' GRBs ($L \leq 10^{49}$ ergs^{-1}) barely need the correction for beaming, and therefore we can infer that they emit almost isotropically. This result is in good agreement with observations (admittedly on scanty statistics). For example, for GRB 060218, Soderberg et al. (2006) find $\theta > 70^\circ$; for GRB 031203, $\theta > 30^\circ$ (Malesani, private communication); and for the 'low-luminosity' GRB population (Guetta & Della Valle 2007) $\theta > 25^\circ$ (corresponding to $f_b^{-1} \leq 10$) . The increasing ratio GRB/SN Ib/c $\sim 10^{-3}$–10^{-2} for $z \sim 1$, in the case of the Matsubayashi et al. (2005) GRB rate, may suggest either a different behaviour for 'cosmological' GRBs owing to the existence of a different GRB population (e.g. Bromberg, Nakar & Piran 2011, and references therein) characterized by a larger beaming factor, probably of the order of $f_b^{-1} \sim 20$–200 (corresponding to a jet opening angle of $\sim 20^\circ$–6°), or that the Matsubayashi et al. semi-empirical track is still affected by the obvious bias that favours the discovery at high redshift of only highly beamed GRBs. Similar conclusions (short of a constant) can be obtained by comparing the SN Ib/c rate track with the GRB track by Wanderman & Piran (2010) and with that by Salvaterra et al. (2012). In particular, the Salvaterra et al. (2012) rate is derived from a redshift complete sample of bright Swift GRBs under the assumption that GRBs did not experience luminosity evolution with redshift. It is worth noting that on the basis of the current studies, it is not possible to distinguish between a pure density and a pure luminosity evolution. In general, there is no agreement among authors on this issue. Butler, Bloom & Poznanski (2010) suggest that pure density evolution models produce the observed number of GRBs at high redshift, but in other works the luminosity evolution is used to explain the GRB rate (e.g. see Salvaterra et al. 2009b; Petrosian, Bouvier & Ryde 2009) increasing faster than some CSFR, such as that of Hopkins & Beacom (2006). This is because the Hopkins & Beacom (2006) CSFR decreases at high redshift. However, this behaviour of the CSFR needs to be confirmed by more data, and at the moment we cannot exclude the CSFR being flat at high redshift.

6 CONCLUSIONS

In this paper we have computed the SN Ib/c rates expected at the present time in irregular and spiral galaxies of various masses with the aim of predicting the variation with redshift of the SN Ib/c rate based on successful models for the chemical evolution of irregulars and spirals. We considered both single WR stars and massive stars in binary systems as SN Ib/c progenitors. We used stellar evolution results indicating that the minimum mass of WR stars is a function of the stellar metallicity, thus suggesting a higher rate of SNe Ib/c in more metal-rich galaxies. Then we considered various CSFRs as functions of cosmic time, both theoretically and observationally derived, and computed the cosmic SN Ib/c rates expected from the assumptions on SN Ib/c progenitors. These cosmic SN Ib/c rates were then compared with the observationally derived cosmic GRB rate. Our main conclusions can be summarized as follows.

(i) By taking into account WR progenitors depending on the metallicity and a fraction of massive close binary systems equal to 15 per cent of all massive stars as SN Ib/c progenitors, it is possible to reproduce the present observed SN Ib/c rate both in dwarf metal-poor irregular and in spiral galaxies. It is worth noting that the galactic evolution models adopted here reproduce well the main chemical properties of these galaxies.

(ii) If a dependence on stellar metallicity is assumed for the WR stars, differences arise in the SN Ib/c rates only at early evolutionary times in galaxies. Negligible differences are produced on the predicted local rates.

(iii) We compared the local observed Type Ib/c rates in spirals and irregulars with the local GRB rate and derived a local ratio GRB/SNe Ibc of $\sim 3 \times 10^{-3}$. As expected, only a fraction of these SNe give rise to GRBs.

(iv) We took various CSFR histories and computed the cosmic SN Ib/c rates. Also in this case we considered both a constant minimum WR mass and a mass varying with metallicity. The effect of the dependence of $M_{\rm WR}$ on the metallicity is to predict lower cosmic SN Ib/c rates at very high redshifts. We then compared the cosmic SN Ib/c rates with the cosmic GRB rate derived from Swift data and found that the ratio GRB/SNe Ibc $\sim 10^{-4}$. This confirms previous results that only a small fraction of all SNe Ib/c give rise to GRBs, but our factor is smaller than that found in Bissaldi et al. (2007). The reason for this resides in the fact that we adopted the recent GRB cosmic rate derived from Swift data, whereas in Bissaldi et al. (2007) the cosmic GRB rate was derived on the basis of semi-empirical estimates (Matsubayashi et al. 2005). On the other hand, if we compare our cosmic SN rates with the Matsubayashi et al. (2005) rate we confirm the results of Bissaldi et al. (2007), indicating a ratio of GRB/SN Ib/c rates of $\sim 10^{-3}$–10^{-2}.

(v) Studies of GRBs and their hosts have been shown to be extremely important in tracing galactic evolution at very high redshifts, although the interpretation of cosmic diagrams is difficult as it involves assumptions on the luminosity function of both galaxies and GRBs. It is interesting to note that Salvaterra & Chincarini (2007) pointed out that by adopting the CSFR derived by Cole et al. (2001) and assuming a GRB luminosity function independent of redshift, the number of high-redshift GRBs detected by Swift is largely underestimated. This fact could be interpreted in two ways: either the characteristic luminosity of GRBs increases with redshift, or the CSFR at very high redshifts is higher than in Cole et al. (2001). We have shown that a high CSFR can be achieved by means of monolithic-like models of ellipticals producing stars at a very high rate and at very high redshifts. However, no firm conclusions can be drawn on the CSFR at very high redshifts because of the large uncertainties caused by dust corrections.

ACKNOWLEDGMENTS

VG thanks Anahí Granada, Cyril Georgy and Luca Vincoletto for many useful discussions.

REFERENCES

Asplund M., Grevesse N., Sauval A. J., Scott P., 2009, ARA&A, 47, 481
Baron E., 1992, MNRAS, 255, 267
Berger E., Penprase B. E., Cenko S. B., Kulkarni S. R., Fox D. B., Steidel C. C., Reddy N. A., 2006, ApJ, 642, 979
Bissaldi E., Calura F., Matteucci F., Longo F., Barbiellini G., 2007, A&A, 471, 585
Blanc G., Greggio L., 2008, Nat, 13, 606
Boissier S., Prantzos N., 1999, MNRAS, 307, 857
Boissier S., Prantzos N., 2009, A&A, 503, 137
Bradamante F., Matteucci F., D'Ercole A., 1998, A&A, 337, 338
Bromberg O., Nakar E., Piran T., 2011, ApJ, 739, L55
Butler N. R., Bloom J. S., Poznanski D., 2010, ApJ, 711, 495
Calura F., Matteucci F., 2003, ApJ, 596, 734
Calura F., Matteucci F., 2004, MNRAS, 350, 351
Calura F., Matteucci F., 2006, ApJ, 652, 889
Calura F., Matteucci F., Menci N., 2004, MNRAS, 353, 500
Calura F., Pipino A., Chiappini C., Matteucci F., Maiolino R., 2009, A&A, 504, 373
Campisi M. A., Tapparello C., Salvaterra R., Mannucci F., Colpi M., 2011, MNRAS, 417, 1013
Chiappini C., Matteucci F., Gratton R., 1997, ApJ, 477, 765
Chiappini C., Matteucci F., Romano D., 2001, ApJ, 554, 1044
Chomiuk L., Povich M. S., 2011, AJ, 142, 197
Cole S. et al., 2001, MNRAS, 326, 255
Conselice C. J. et al., 2005, ApJ, 633, 29
Erb D. K., Shapley A. E., Pettini M., Steidel C. C., Reddy N. A., Adelberger K. L., 2006, ApJ, 644, 813
Frail D. A. et al., 2001, ApJ, 562, L55
Fruchter A. S. et al., 2006, Nat, 441, 463
Fukugita M., Hogan C. J., Peebles P. J. E., 1998, ApJ, 503, 518
Fynbo J. P. U. et al., 2003, A&A, 406, L63
Fynbo J. P. U. et al., 2006, A&A, 451, L47
Georgy C., Meynet G., Walder R., Folini D., Maeder A., 2009, A&A, 502, 611
Gorosabel J. et al., 2005, A&A, 444, 711
Guetta D., Della Valle M., 2007, ApJ, 657, L73
Guetta D., Piran T., Waxman E., 2005, ApJ, 619, 412
Hamuy M., 2002, preprint (astro-ph/0301006)
Harris J., Zaritsky D., 2009, AJ, 138, 1243
Hjorth J., Bloom J. S., 2011, in Kouveliotou C., Wijers R. A. M. J., Woosley S. E., eds, Gamma-ray Bursts. Cambridge Univ. Press, Cambridge
van den Hoek L. B., Groenewegen M. A. T., 1997, A&AS, 123, 305
Hopkins X., 2004, ApJ, 615, 209
Hopkins A. M., Beacom J. F., 2006, ApJ, 651, 142
Iwamoto K. et al., 1998, Nat, 395, 672
Iwamoto K., Brachwitz F., Nomoto K., Kishimoto N., Umeda H., Hix W. R., Thielemann Friedrich-K., 1999, ApJS, 125, 439
Jeffries R. D., Maxted P. F. L., 2005, Astron. Nachr., 326, 944
Kewley L. J., Ellison S. L., 2008, ApJ, 681, 1183
Kistler M. D., Yüksel H., Beacom J. F., Hopkins A. M., Wyithe J. S. B., 2009, ApJ, 705, L104
Kobulnicky H. A., Fryer C. L., 2007, ApJ, 670, 747
Krühler T. et al., 2011, A&A, 534, 108
Lee H., Skillman E. D., Cannon J. M., Jackson D. C., Gehrz R. D., Polomski E. F., Woodward C. E., 2006, ApJ, 647, 970
Li L.-X., 2008, MNRAS, 388, 1487
Li W., Chornock R., Leaman J., Filippenko A. V., Poznanski D., Wang X., Ganeshalingam M., Mannucci F., 2011, MNRAS, 412, 1473
MacFayden A., Woosley S., 1999, ApJ, 524, 262
MacLow M. M., Ferrara A., 1999, ApJ, 513, 142
Madau P., Della Valle M., Panagia N., 1998, MNRAS, 297, L17
Maiolino R. et al., 2008, A&A, 488, 463
Mannucci F., Della Valle M., Panagia N., Cappellaro E., Cresci G., Maiolino R., Petrosian A., Turatto M., 2005, A&A, 433, 807
Mannucci F., Salvaterra R., Campisi M. A., 2011, MNRAS, 414, 1263
Martin C. L., 1999, ApJ, 513, 156
Martin C. L., Kobulnicky H. A., Heckman T. M., 2002, ApJ, 574, 663
Marzke R. O., Geller M. J., Huchra J. P., Corwin H. G., Jr, 1994, AJ, 108, 437
Matsubayashi T., Yamazaki R., Yonetoxu D., Murakami T., Ebisuzaki T., 2005, Prog. Theor. Phys., 114, 983
Matteucci F., 2001, Nat, 414, 253
Matteucci F., François P., 1989, MNRAS, 239, 885
Modjaz M. et al., 2008, AJ, 135, 1136
Paczyǹski B., 1998, ApJ, 494, L45
Petrosian V., Bouvier A., Ryde F., 2009, pre-print (arXiv:0909.5051)
Pipino A., Matteucci F., 2004, MNRAS, 347, 968
Podsiadlowski Ph., Josh P. C., Hsu J. J. L., 1992, ApJ, 391, 246
Porciani C., Madau P., 2001, ApJ, 548, 522
Prantzos N., Boissier S., 2003, A&A, 406, 259
Prieto J. L., Stanek K. Z., Beacom J. F., 2008, ApJ, 673, 999
Prochaska J. X. et al., 2004, ApJ, 611, 200
van Putten M. H. P. M., Regimbau T., 2003, ApJ, 593, L15
Salpeter E. E., 1955, ApJ, 121, 1615
Salvaterra R., Chincarini G., 2007, ApJ, 656, L49
Salvaterra R. et al., 2009a, Nat, 461, 1258
Salvaterra R., Guidorzi C., Campana S., Chincarini G., Tagliaferri G., 2009b, MNRAS, 396, 299
Salvaterra R. et al., 2012, ApJ, 749, 68
Savaglio S., 2006, New J. Phys., 8, 195
Savaglio S. et al., 2005, ApJ, 635, 260
Savaglio S., Glazebrook K., Le Borgne D., 2009, ApJ, 691, 182
Schmidt M., 1959, ApJ, 129, 2435
Schechter P., 1976, ApJ, 203, 2975
Schmidt X., 2001, ApJ, 552, 36
Smartt S. J., 2009, ARA&A, 47, 63
Smith N., Li W., Filippenko A. V., Chornock R., 2011, MNRAS, 412, 1522
Soderberg A. M. et al., 2004, ApJ, 606, 994
Soderberg A. M. et al., 2006, Nat, 442, 1014
Spitoni E., Matteucci F., Recchi S., Cescutti G., Pipino A., 2009, A&A, 531, 72
Stanek K. Z. et al., 2006, Acta Astron., 56, 333
Steidel C. C., Adelberger K. L., Giavalisco M., Dickinson M., Pettini M., 1999, ApJ, 519, 15
Strolger L. G. et al., 2004, ApJ, 613, 200
Tanvir N. R., Levan A. J., 2007, preprint (arXiv:0709.0861)
Tanvir N. R. et al., 2009, Nat, 461, 1254
Tremonti C. A. et al., 2004, ApJ, 613, 898
Wainwright C., Berger E., Penprase B. E., 2007, ApJ, 657, 367
Wanderman D., Piran T., 2010, MNRAS, 406, 1944
Wolf C., Podsiadlowsky P., 2007, MNRAS, 375, 1049
Woosley S. E., 1993, ApJ, 405, 273
Woosley S. E., Bloom J. S., 2006, ARA&A, 44, 507
Woosley S. E., Weaver T. A., 1995, ApJS, 101, 181
Yin J., Magrini L., Matteucci F., Lanfranchi G. A., Gonçalves D. R., Costa R. D. D., 2010, A&A, 520, 55
Yonetoku D., Yamazaki R., Nakamura T., Murakami T., 2005, MNRAS, 362, 1114
Yoon S.-C., Woosley S. E., Langer N., 2010, ApJ, 725, 940
Zhang B., Woosley S. E., MacFayden A. I., 2003, ApJ, 586, 356

This paper has been typeset from a TEX/LATEX file prepared by the author.